Geophys. J. Int. (2007) **169,** 917–925 doi: 10.1111/j.1365-246X.2007.03326.x

The dynamics of magnetic ordering in a natural hemo-ilmenite solid solution

A. U. Gehring,[1] H. Fischer,[1] E. Schill,[2] J. Granwehr[3] and J. Luster[4]

[1] *Institute of Geophysics, ETH Zurich,* 8093 *Zurich, Switzerland. E-mail: gehring@sl.ethz.ch*
[2] *Institute of Geosciences—Geophysics und Geodynamics, Johannes Gutenberg University of Mainz,* 55099 *Mainz, Germany*
[3] *Sir Peter Mansfield Magnetic Resonance Centre, School of Physics and Astronomy, University of Nottingham, Nottingham* NG7 2RD, *UK*
[4] *Swiss Federal Institute for Forest, Snow, and Landscape Research WSL,* 8903 *Birmensdorf, Switzerland*

Accepted 2006 December 6. Received 2006 September 7; in original form 2006 April 3

SUMMARY

We investigated the micromagnetic properties of hemo-ilmenite particles in an alluvial soil. All magnetic accessory minerals except the weathering resistant hemo-ilmenite grains were removed from the soil matrix by chemical treatment with concentrated acid followed by magnetic separation. X-ray diffraction revealed hemo-ilmenite grains with single crystal properties and an ilmenite mole fraction of $y = 0.86$. Magnetization versus applied magnetic field plots in a temperature range between 6 and 300 K were recorded in order to study the hysteresis and the exchange properties. In addition, field and frequency-dependent AC susceptibility measurements were performed with and without a DC bias field in order to analyse the dynamic magnetization of the sample down to 3 K.

The hemo-ilmenite particles are considered as a mixed system with nano-sized cation-ordered areas (COA) and cation-disordered areas (CDA), which differ in their local $Fe^{(III)}$ concentration. Ferrimagnetic single-domain order in the $Fe^{(III)}$-enriched CDA started at about 220 K. Upon cooling gradual transdomain transformation generates multidomain order. A maximum in the blocking distribution was reached at 44 K, followed by the onset of spin-glass dynamics. At lower temperature, blocking of superparamagnetic clusters in the COA created antiferromagnetic (AFM) ordering, which became more prominent with decreasing temperature. The interaction between the spin-glass like CDA and the AFM areas was documented by the onset of exchange bias at $T < 20$ K. The occurrence of exchange bias as well as spin-glass dynamics in the hemo-ilmenite grains is probably an effect of the inhomogeneity of the local $Fe^{(III)}$ concentration. This effect leaves a magnetically competitive regime with areas showing ilmenite-like magnetic properties, and $Fe^{(III)}$ rich disordered areas with magnetic long-range ordering up to 220 K and frustration near the ordering temperature of ilmenite.

Key words: environmental magnetism, exchange anisotropy, hemo-ilmenite, low-temperature magnetism, solid solution, superparamagnetic clusters.

1 INTRODUCTION

Mineral phases of the hematite–ilmenite solid solution series (y $FeTiO_3$ – (1-y) α-Fe_2O_3; $0 < y < 1$) belong to the most abundant and chemically stable accessory constituents in rocks. They can play an important role in rock magnetism, and they can be used as magnetic proxy in the reconstruction of weathering regimes (e.g. McEnroe *et al.* 2002; Schroeder *et al.* 2002). Furthermore, this solid solution series which comprehends antiferromagnetic (AFM) insulators as well as semi-conducting, ferrimagnetic (FM) phases, has been considered for potential applications in spintronics (e.g. Fujii *et al.* 2005).

The end-members have a rhombohedral crystal structure and are AFM with Néel temperatures of 948 K for hematite and of 54 K for ilmenite (Ishikawa *et al.* 1985).

The hematite crystal structure consists of stacked sheets of octahedrally coordinated $Fe^{(III)}$ between two closed-packed layers of oxygens. The symmetry is higher than the one of the ilmenite structure with $Fe^{(II)}$ and $Ti^{(IV)}$ cations separated into two sublattices. The substitution of $Fe^{(II)} + Ti^{(IV)}$ for $Fe^{(III)}$ as the composition departs from hematite takes place randomly. At ilmenite-rich composition ($y > 0.5$) the substituting cations become ordered so that alternating cation layers are no longer equivalent, the Ti^{4+} being confined to alternate layers (e.g. Brown *et al.* 1993; Harrison & Redfern 2001). As a result, boundary layers (e.g. twinning planes) can be formed if adjacent cation layers of two ordered phases are not matched (e.g. Lawson *et al.* 1981). In a first approximation, the magnetic ordering temperature of the solid solutions exhibits a linear increase with an increasing mole fraction of α-Fe_2O_3 (Nagata & Akimoto 1956). Ilmenite-rich solid solutions ($1 > y > 0.5$) considered as

hemo-ilmenite, reveal FM ordering. Furthermore, the low-temperature magnetic properties of synthetic hemo-ilmenite solid solutions with y between 0.79 and 0.9 were interpreted as showing spin glass behaviour (Arai *et al.* 1985; Ishikawa *et al.* 1985).

Transmission electron microscopy and micromagnetic investigations showed that hemo-ilmenites ($y > 0.5$) are magnetically inhomogeneous and consist of cation-ordered FM microstructures which are separated by boundary layers (e.g. Nord & Lawson 1992). Based on crystallographic considerations it is supposed that the $Fe^{(III)}$-enriched boundary layers have an AFM ordering (e.g. Lawson *et al.* 1981). It is expected that these boundary layers play a key role in the onset of intrinsic magnetic properties such as the self-reversal of thermoremanence (e.g. Nord & Lawson 1992; Prévot *et al.* 2001; Lagroix *et al.* 2004; Harrison *et al.* 2005). Boundary layers, i.e. cation-disordered areas (CDA), however, are difficult to investigate directly because they are often nano-sized and metastable and their magnetic properties are masked by the magnetic ordering of the adjacent cation-ordered areas (COA). An indirect way to get an insight into the magnetization properties of boundary layers can be attained through their exchange interactions with the FM phase. For example, Meiklejohn & Carter (1959) found a slight shift of the hysteresis loop of hemo-ilmenite ($y = 0.6$) which provided clear evidence for an exchange coupling between a FM and an AFM phase.

The brief review above of studies on mainly synthetic materials demonstrates that mixed-valence oxides can have a complex magnetic nanoscale structure. However, little is known on how the nanostructures affect the magnetic behaviour of natural multimineral materials containing such oxides. A better understanding of such interactions can strongly improve the use of magnetic properties to reconstruct erosion processes, pedogenesis and diagenetic processes in sedimentary environments. In particular, results obtained with synthetic hemo-ilmenites can be applied to natural systems only to a certain extent because the proportion of the cation-disordered boundary layers is larger in the latter (Prévot *et al.* 2001). Nonetheless, they provide an invaluable framework to classify and interpret results obtained with natural samples.

The purpose of this research is to study the micromagnetic properties of a natural hemo-ilmenite with special attention to the interaction between the COA and CDA. We use a soil sample in which all magnetic accessory minerals except the weathering resistant hemo-ilmenite were removed in order to minimize the superposition of magnetic signals.

2 SAMPLES AND METHODS

The studied hemo-ilmenite is a lithogenic component derived from a volcanic parent rock deposited in an alluvial Vertisol in southern Mali. The μ-sized hemo-ilmenite grains are dispersed in the soil matrix which mainly consists of paramagnetic (PM) montmorillonite, diamagnetic quartz, and some magnetite as FM impurity (Gehring *et al.* 1997). The magnetic experiments were carried out with topsoil samples (Ap horizon) dried at 60°C and passed through a 2-mm sieve. In order to remove all iron oxides except ilmenite, the samples were acid treated followed by magnetic separation. The chemical treatment included boiling the sample in concentrated acid solution with a 19:1 ratio of HCl to H_2SO_4 (Goulart *et al.* 1994). After this treatment the bulk samples contained no mineral phase carrying a remanent magnetization at room temperature. The mineralogical identification of the hemo-ilmenite was performed by scanning electron microscopy (SEM) and by single crystal X-ray diffraction (CAD-4 diffractometer with $Cu_{K\alpha}$ radiation) on hand picked grains ($n = 4$).

Magnetic measurements between 3 and 300 K were performed on acid-treated bulk soil samples in order to determine the magnetic properties of the hemo-ilmenite. Hysteresis behaviour of the magnetization as a function of the magnetic field up to 1 Tesla between room temperature and 6 K were measured with a vibrating sample magnetometer (VSM, Princeton Measurements) equipped with a helium cryostat. All loops were started in a 1 T field and the elapsed time for one cycle was 105 s with measuring steps of 10 mT. The hysteresis loops were 70 per cent slope corrected for the PM constituents in the soil samples. In order to obtain a better insight into the correlation between magnetic interactions, expressed as B_b, and the distribution of the coercivity, B_c, in the solid solution, first-order reversal curve (FORC) diagrams were determined (Pike *et al.* 1999; Roberts *et al.* 2000). The curves were recorded in a temperature range between 240 and 30 K. The FORC data were processed with a Matlab code by Winkelhofer and Pike (Winkelhofer, personal communication, 2006). For all diagrams a smoothing factor of 3 was used.

The AC susceptibility measurements were used in order to study the dynamic response of the sample magnetization and to identify magnetic transitions in the hemo-ilmenite grains. Both the in-phase (χ') and the out-of-phase susceptibility (χ'') were analysed. The χ' responds to all non-saturated phases which include the PM clay minerals of the matrix. By contrast, χ'' indicates dissipative processes in the sample, for example irreversibility or relaxation with a time constant that has a similar order of magnitude as the inverse of the AC frequency. The AC susceptibility measurements were carried out using a Quantum Design PPMS (Physical Property Measurement) at amplitude fields (B_{ac}) between 0.1 and 1.2 mT and frequencies in a range between 10 Hz and 10 kHz with or without a superimposed 1 T DC field.

3 RESULTS

3.1 Mineralogical properties of hemo-ilmenite grains

Under the SEM the hemo-ilmenite showed a typical grain size between 50 and 100 μm which was similar to the one of the quartz grains. The shape of the grains varied and it occasionally resembled the hexagonal crystal lattice symmetry (Fig. 1). The XRD pattern of the grains revealed a coherent structure typical for single crystals. The symmetry of the crystal was $R\overline{3}$, which is characteristic for the ilmenite structure. The hexagonal unit cell parameters were $a = 5.075 \pm 0.001$ Å and $c = 14.041 \pm 0.001$ Å, and the volume of the unit cell was 313.3 Å^3. Using the relationship between the unit cell volume and the mole fraction of ilmenite in hematite-ilmenite solid solutions by Brown *et al.* (1993), a $y = 0.86$ was deduced for the single crystal grains in the soil. With this information the equation by Nagata & Akimoto (1956) can be adopted, which describes the relation between chemical composition and magnetic ordering temperature; a Curie temperature (T_c) of about 200 K was determined for the FM hemo-ilmenite grains.

3.2 Low field susceptibility

The low field susceptibility as a function of temperature exhibited an in-phase and an out-of-phase component with diverse frequency and amplitude dependencies. At room temperature, a small positive value of χ' near the detection limit is probably partially caused by

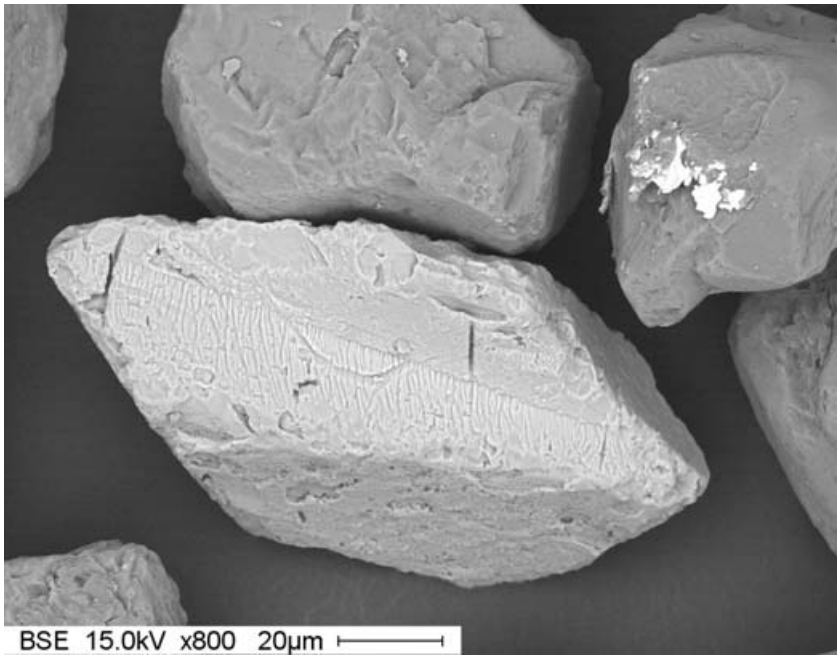

Figure 1. Scanning electron micrograph of a handpicked hemo-ilmenite grain surrounded by quartz grains. The white flakes on the surface of the quartz grain to the right are native gold.

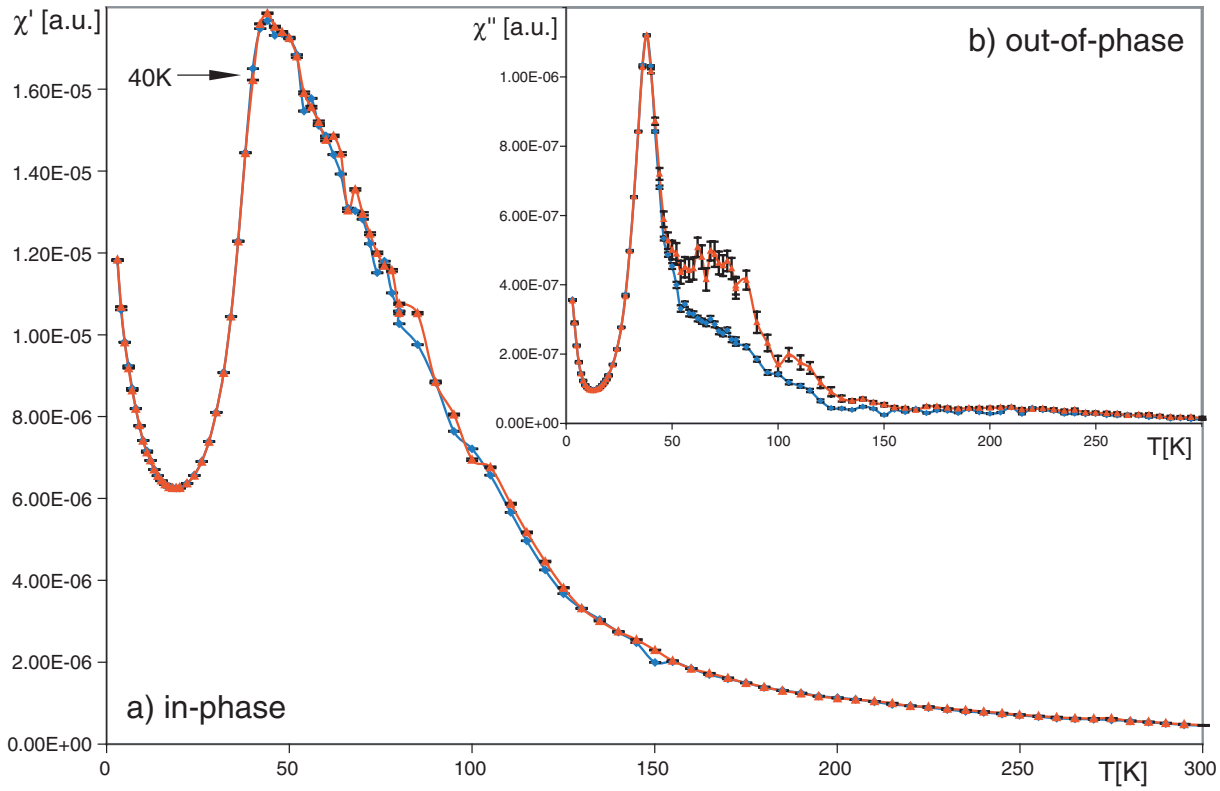

Figure 2. Variation of the low-field AC susceptibility between 3 and 300 K with an in-phase (a) and an out-of-phase (b) component at 1 kHz frequency and amplitudes of 1.2 mT (red triangles) and 0.3 mT (blue dots). The lowest temperature with amplitude dependence is arrowed.

PM minerals in the bulk soil material. In the amplitude range of 0.1 and 1.2 mT and at a constant frequency of 1 kHz, a distinct increase of χ' was observed at about 180 K and a maximum was reached at 44 K. The subsequent drop was followed by a second increase at 20 K, which reached no maximum down to 3 K (Fig. 2a). The temperature dependence of the AC susceptibility was nearly identical for cooling and warming. A weak response of χ' to changing B_{ac} was observed between about 150 and 40 K. The out-of-phase

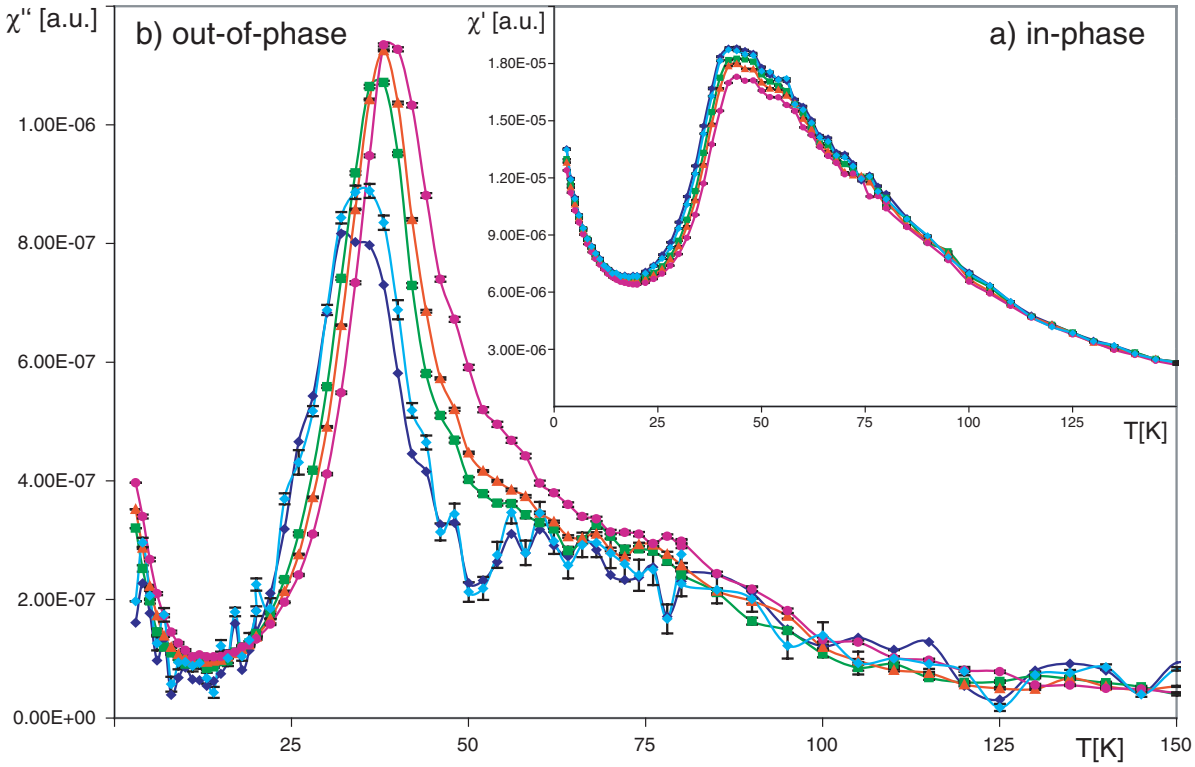

Figure 3. Variation of the low-field AC susceptibility between 3 and 150 K with an in-phase (a) and an out-of-phase (b) component for the frequencies of 45 Hz (dark blue diamonds), 90 Hz (light blue diamonds), 450 Hz (green squares), 1000 Hz (orange triangles) and 4500 Hz (purple dots) and an amplitude of 0.3 mT.

component revealed a distinct increase at about 130 K, a shoulder around 70 K, and a peak at 38 K (Fig. 2b). This was followed by a drop to a local minimum at 13 K and another increase without reaching a maximum at 3 K. The shoulder at 70 K revealed clear amplitude dependence. At $T < 40$ K this dependence disappeared. Frequency dependence of χ' occurred between about 100 and 3 K and was more pronounced between 56 and 23 K (Fig. 3a). No significant frequency-dependent shift of the maximum at about 44 K was observed. The steep flank, however, at $T < 44$ K revealed a clear shift towards lower temperature with lowering the frequency. The same trend was found for the peak of the χ'' at 38 K. Furthermore, the intensity of this peak enhanced with increasing frequency (Fig. 3b). The frequency dependence of χ'' started at about 60 K. The amplitude dependence was complementary to the frequency dependence, with the broad field-dependent shoulder at about 70 K (Fig. 2b) flanking the frequency-dependent peak (Fig. 3a).

A DC bias field reduces both the χ' and χ'' AC component. The inverse χ' was not linear with decreasing temperature, indicating that it originated not only from the PM constituents in the matrix. The non-zero χ'' showed a distinct increase below 38 K with a shoulder at about 25 K and a subsequent steep increase down to 3 K (Fig. 4). At $T < 20$ K, the χ'' was similar with and without 1 T DC bias field, indicating that its origin was either a PM or an ordered phase that was not saturated at 1 T.

3.3 Hysteresis properties

Hysteretic behaviour of the soil sample, which was weak and therefore rather noisy, occurred upon cooling to 200 K. Further cooling to 30 K led to the hysteresis loop closures at fields less than 0.8 T (Figs 5a and b). In this temperature range, the remanent magnetization (M_r) exhibited a steady increase whereas the M_r to saturation magnetization (M_s) ratio decreased upon cooling from $M_r/M_s = 0.3$ at 220 K, which is typical for pseudo-single domain (PSD) structures, to $M_r/M_s = 0.12$, indicating multidomain areas, at 80 K. The M_r/M_s ratio remained stable down to 40 K, and increased anew at lower temperature (Figs. 6a and b). Above 40 K, the coercivity (B_c) revealed a maximum of 32 mT at 150 K and a minimum of 13.9 mT at 50 K (Fig. 6c). The hysteresis loops between 150 and 30 K (Fig. 5b) were wasp-waisted, i.e. the width of the loop narrowed as magnetization went to zero. This behaviour became more pronounced with decreasing temperature.

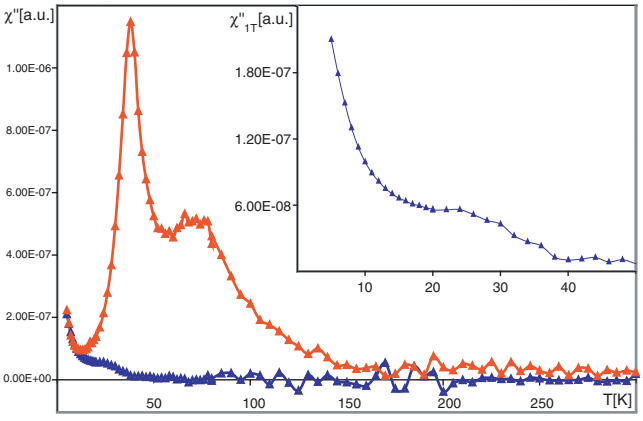

Figure 4. Comparison of the temperature dependence of the out-of-phase AC susceptibility at 1 kHz and an amplitude of 1.2 mT without (red triangle) and with (blue triangle) a DC bias field of 1T. Inlet shows the blow up of the χ'' in a 1T bias field (χ''_{1T}) between 50 and 5 K.

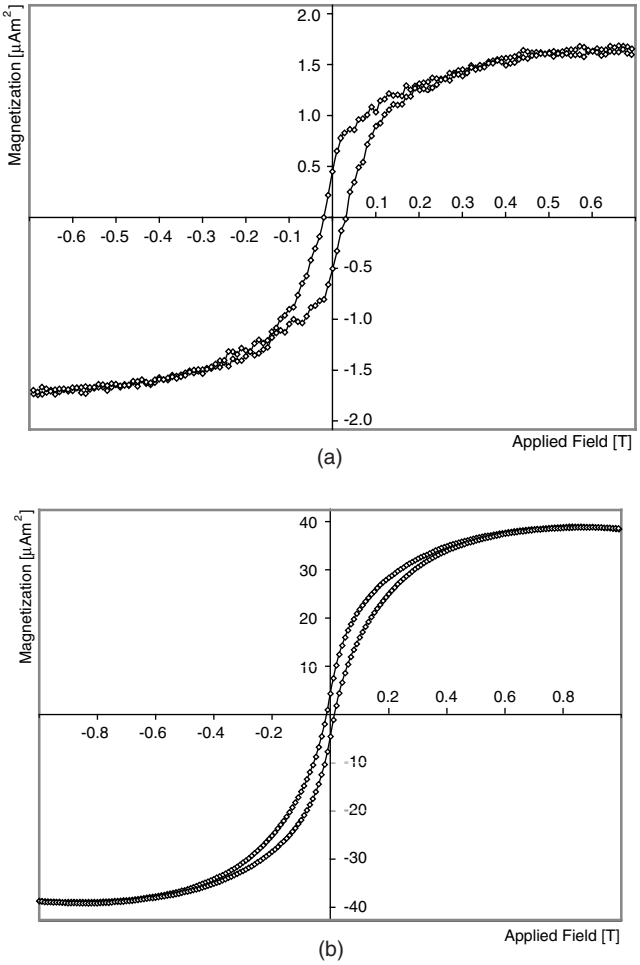

Figure 5. Hysteresis loops at 200 K (a) and 45 K (b). The loops are 70 per cent slope corrected for the PM matrix components.

The FORC contour plot at 200 K revealed an elongated distribution along the B_c axis (Fig. 7a). Such a feature is characteristic for single domain (SD) or PSD structures, possibly with a second contribution from non-interacting SP clusters. At 150 K, where B_c exhibits in the hysteresis loop a local maximum, the FORC contour plot shows two features, one with a spread along B_c and another with a distribution along the B_b axis at $B_c < 4$ mT (Fig. 7b). Upon further cooling the latter became more pronounced and at 45 K it was dominant and masked the contours along the B_c axis (Fig. 7c). Such a feature could be attributed to superparamagnetic (SP) particles (e.g. Roberts *et al.* 2000). Plotting the FORC distribution for $B_c > 10$ mT without the reversal ridge revealed a relatively narrow distribution along B_c (Fig. 7d), which is indicative of multidomain structures.

The hysteresis loops at $T < 30$ K showed a substantial change in the hysteretic properties (Fig. 6). At 20 K the hysteresis curve revealed $B_c = 92$ mT, the closure of the loop at $B = 0.9$ mT, and a minor shift towards negative fields (Fig. 8a). Such a shift is known as exchange bias (e.g. Nogués & Schuller 1999). The exchange field (B_{ex}) of this shift was 6 mT. At lower temperature, the hysteresis curves were not closed in a maximum 1T field, hinting at the presence of an ordered magnetic phase which had not reached saturation (Fig. 8b). The hysteresis loop at 15 K exhibited $B_c = 144$ mT and $B_{ex} = 7$ mT. At 6 K, B_c reached 244 mT and B_{ex} was 40 mT (Fig. 8b). One has to be aware that the slope correction of the unsaturated

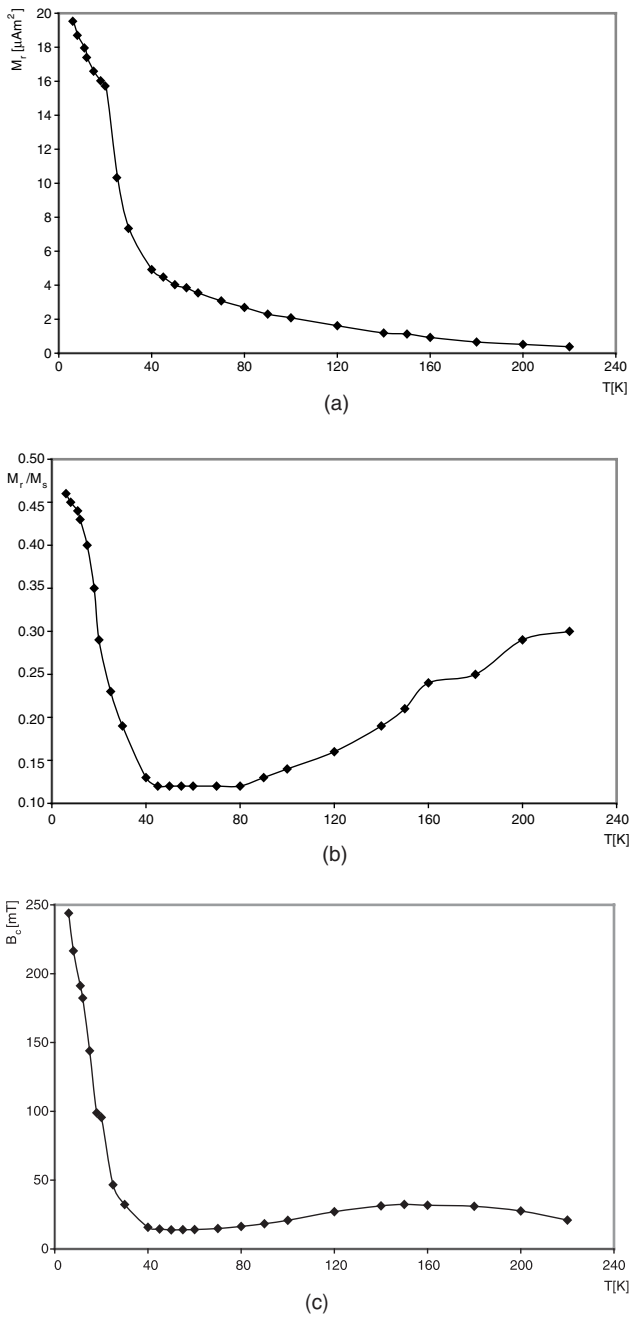

Figure 6. Hysteresis parameters M_r (a), M_r/M_s (b) and B_c (c) versus temperature.

system enhances the effect of the exchange bias, since $B_{ex} = 5$ mT at 15 K and $B_{ex} = 22$ mT at 6 K was found for the uncorrected hysteresis curves.

4 DISCUSSION

Dark-field transmission electron micrographs of natural hemo-ilmenite crystals provide clear evidence for a nanostructured system with cation-ordered domains and a cation-disordered matrix which are different in their local $Fe^{(III)}$ concentration (Prévot *et al.* 2001). Since the two structures have different magnetic properties, hemo-ilmenite solid solutions can be roughly considered as dynamic systems of interacting magnetic nanostructures. Based on the XRD

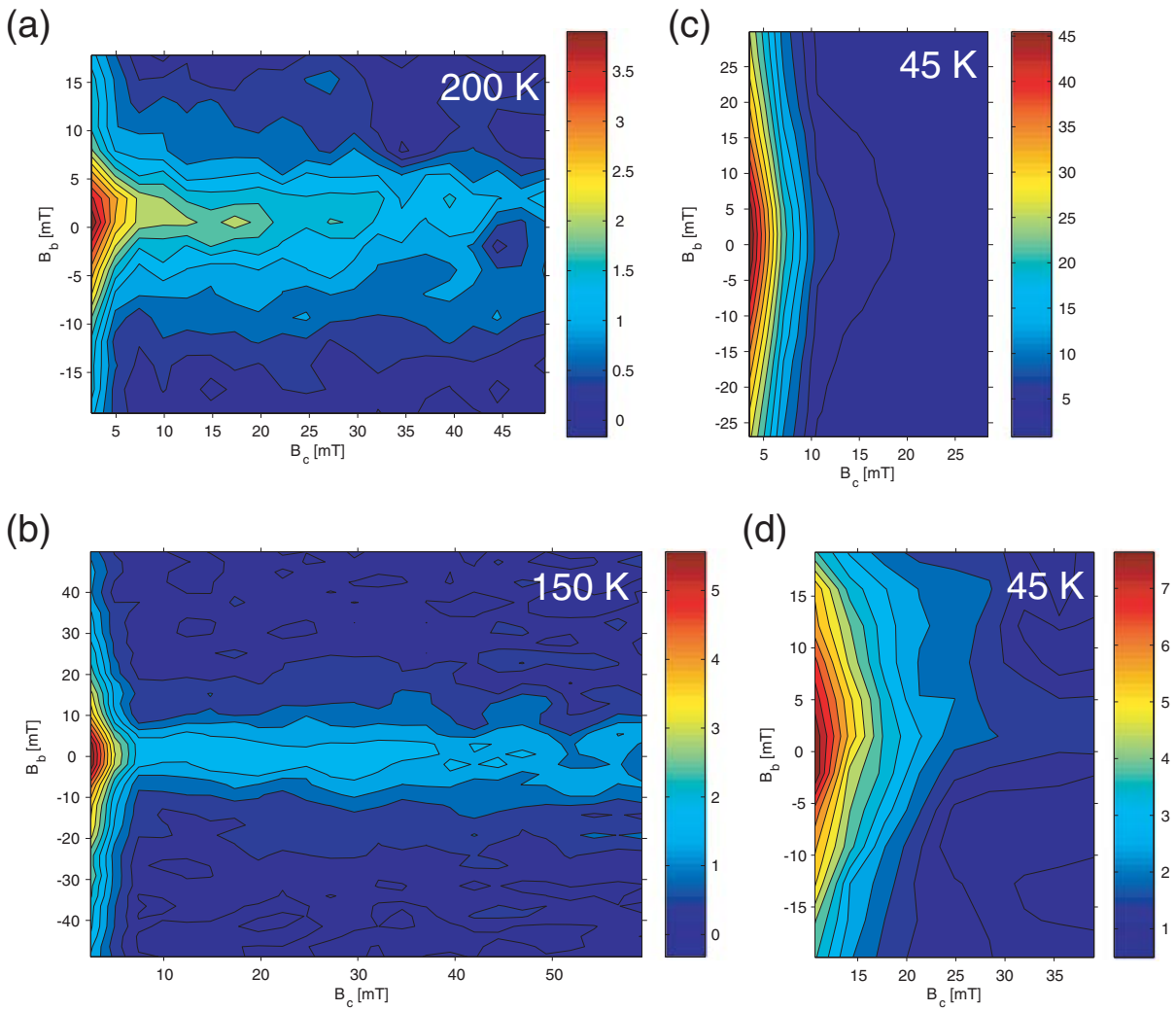

Figure 7. FORC diagram of the soil sample at 200 K (a), 150 K (b) and 45 K (c). In addition, a magnified part of the latter at $B_c > 10$ mT is shown to emphasise the feature along the B_c axis. $B_c > 10$ mT (d). The color scale represents the values for the FORC distribution in arbitrary units.

data, which exhibit single crystal properties for the hemo-ilmenite grains and taking the observation by Prévot *et al.* (2001) into account, we consider in the following the mineralogical structure of the hemo-ilmenite as a mixture of nano-sized COA and CDA, with the latter being $Fe^{(III)}$ enriched.

A hysteresis loop in the M against B plot at 220 K indicates the generation of a magnetically ordered phase. Considering this temperature as the T_c of the hemo-ilmenite agrees well with the $y = 0.86$ and the derived $T_c = 200$ K deduced from the X-ray data.

Ishikawa *et al.* (1985) reported two different types of spin-glass properties for synthetic single crystal hemo-ilmenite with y-values between 0.9 and 0.79. The one with $y \approx 0.8$ was described as re-entrant spin-glass. In such a phase, the low-field magnetization exhibits an increase below $T_c = 220$ K followed by a decrease below 100 K towards zero, which indicates that the spin-glass phase is entered through a FM region. In addition, there was a pronounced increase in B_c and M_r below 50 K. The other synthetic single crystal hemo-ilmenite with $y = 0.9$ was interpreted as cluster-spin-glass phase which is characterized by a $T_c \approx 50$ K, a freezing temperature at 38 K, and an increase in B_c and M_r at $T < 38$ K. In other words, upon cooling this spin-glass dynamics sets in immediately after the FM ordering. The fact that with these homogeneous single crystals the ordering temperature went up significantly with increased $Fe^{(III)}$ content hinted towards an ordering mechanism where $Fe^{(III)}$ ions in $Ti^{(IV)}$ layers align the moments of neighbouring $Fe^{(II)}$ ions, forming a FM cluster (Ishikawa 1964). Our natural sample is structurally not nearly as homogeneous as the synthetic single crystals used to derive these mechanisms, thus a distribution of local $Fe^{(III)}$ concentrations should lead to a distribution of the magnetic ordering over a large temperature range, starting at the temperature where ordering in the re-entrant spin-glass is reported by Ishikawa *et al.* (1985). However, as a common feature it seems plausible that it is the presence of $Fe^{(III)}$ ions that causes the formation of FM clusters at temperatures above the Néel temperature of ilmenite, therefore the CDA block at higher temperatures than the COA. Furthermore, it can be expected that in certain regions the local $Fe^{(III)}$ concentration remains below the threshold concentration for the onset of magnetic ordering other than the AFM blocking of ilmenite.

Considering all this, the temperature dependence of χ' and χ'' can be assigned to hemo-ilmenite grains consisting of two magnetic components with different blocking and saturation behaviours, each of them showing a distribution of the blocking properties as a function of temperature due to varying local $Fe^{(III)}$ concentration and domain size. Since the soil matrix contains PM montmorillonite,

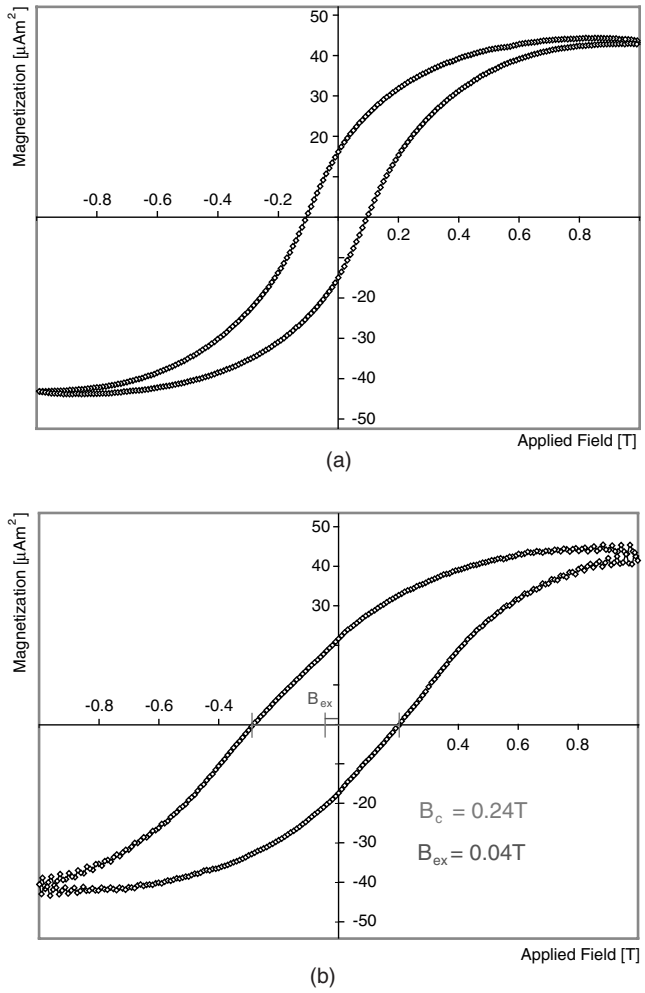

Figure 8. Hysteresis loop at 20 K (a) and 6 K (b). The loops are 70 per cent slope corrected for the PM matrix components. The sample is not saturated in a 1 T field. The exchange bias (B_{ex}) and B_c are indicated.

which could magnetically order at $T < 4$ K (Dickson & Cardile 1986), an unambiguous assignment of the χ' data at very low temperature to the hemo-ilmenite grains cannot be made. Therefore, χ' data at $T < 20$ K are not further discussed. By contrast, a significant fraction of χ'' is most likely due to hemo-ilmenite, since χ'' from PM samples would show different frequency dependence, and the longitudinal relaxation times of PM cations are relatively fast compared to the used AC frequencies. Furthermore, the effect of PM phases on the hysteretic properties can be neglected, because the longitudinal relaxation time of paramagnetic $Fe^{(III)}$ cations even at very low temperature is several orders of magnitude shorter than the circling time of 105 s. For a detailed discussion, the magnetic ordering of the hemo-ilmenite is subdivided into two temperature ranges above and below 40 K.

4.1 Magnetic properties above 40 K

The hysteresis loops indicate the onset of the long-range ordering of FM domains at about 200 K. In hemo-ilmenite solid solution with $y > 0.5$ such FM domains are expected (e.g. Ishikawa *et al.* 1985; Nagata & Akimoto 1956). In addition to the FM domains, ordering of a second nanophase starts at about 150 K. The occurrence of this phase is documented in the hysteresis loop which reveals wasp-waisted properties (Tauxe *et al.* 1996; Bennett & Della Torre 2005).

The trends in M_r, B_c and M_r/M_s could be explained by a domain size effect (*cf.* O'Reilly 1984). The B_c distribution in the FORC contour plots and the decrease of M_r/M_s reveal a trend to increasing domain sizes and a transition from SD/PSD to multidomain upon cooling (Fig. 7). However, it is not very likely that the wasp-waisted loops at $T < 150$ K were generated solely by such an effect, since the hysteresis measurements at 45 K exhibit a relatively narrow B_c distribution and pronounced wasp-waistedness (Figs 5b and 7c). An alternative interpretation for the wasp-waisted loop is the generation of short-range ordered areas in the hemo-ilmenite particles. Such clusters would be in the SP state, therefore, they account for no remanence, and the M_r/M_s ratio decreases. Furthermore, the developing of the M_r/M_s ratio and the minor changes in B_c suggest no significant exchange interactions between the FM bulk and the newly generated clusters upon cooling to 40 K. The formation of SP clusters is also supported by the occurrence of a dominant vertical feature in the FORC contour plots (Fig. 7c) (Roberts *et al.* 2000) and the frequency dependence in the AC susceptibility (Fig. 3) at $T < 100$ K (e.g. Dormann *et al.* 1997). SP clusters relax with a certain life time, which is typically dependent on cluster size or shape, causing the occurrence of χ''. Clusters in a SP range have been reported by Ishikawa (1964) for synthetic hemo-ilmenites with $y > 0.88$. Such a mole fraction is close to the one in the hemo-ilmenite ($y = 0.86$) from our soil sample.

The low field susceptibility yields information about magnetization dynamics of the FM domains and the SP clusters in the hemo-ilmenite despite the fact that the response from these two magnetic structures to AC measurements is superimposed (Figs 2b and 3b). Since hysteretic properties are found above 45 K and M_r monotonically increases from 220 K down to 45 K, the peak in χ' does not mark a transition from a SP to a magnetically ordered phase, but instead it can be considered as the temperature (T_B) where the blocking distribution of the FM domains shows its maximum (Balanda *et al.* 2005). The field-dependence of χ'' mainly at about 70 K is indicative of weak hysteresis which can be explained by irreversible domain wall displacement (Jackson *et al.* 1998). The disappearance of such field dependence close to T_B suggests that at this temperature most of the wall displacements in the cation-disordered FM domains get frozen. Such a mechanism can be referred to as field-blocked thermoremanent magnetization and is explained by the creation of energy barriers hindering wall motions (Dunlop & Xu 1994).

Since the vertical feature in the FORC diagram is not significantly altered at T_B of the FM phase, it is very likely that the nanostructures in the SP state are due to a different phase. Based on the above interpretation, the hemo-ilmenite grains at 40 K are composed of cation-disordered multidomain FM areas and cation-ordered SP clusters.

4.2 Magnetic properties below 40 K

In the temperature range from 40 to 3 K a striking change in the magnetization dynamics is indicated by the lack of an amplitude dependence in χ' and χ'' as well as the frequency-dependant peak in χ'' at 38 K. The vanishing of the amplitude dependence is indicative of frozen domain walls in the FM areas. During freezing hard domain walls are generated, which can be interpreted as areas with a low $Fe^{(III)}$ density and no magnetic long-range ordering above T_B within FM domains. The frequency dependence of χ'' and χ' at

38 K, slightly below T_B, is characteristic for spin-glass dynamics (e.g. Jönsson 2004). Because of the simultaneous occurrence of the two effects, it can be postulated that the freezing of the domain walls and a subsequent onset of long-range ordering causes a competing, overlapping ordering regime that induces disorder and frustration, which manifests itself by spin-glass dynamics in the CDA of the hemo-ilmenite solid solution.

At $T < 38$ K the onset of an out-of-phase component in a 1 T DC bias field (χ''_{1T}) points to a non-saturated phase with long-range magnetic ordering (Fig. 4). The fact that a 1 T DC field suppresses the re-entrant spin-glass properties argues against the spin-glass dynamics in the FM areas generating such a feature in χ''_{1T} at $T <$ 38 K (*cf.* Ishikawa *et al.* 1985). Furthermore FM phases are generally saturated in a 1 T field. Hence, the newly formed phase that blocks in has most likely an AFM ordering. Upon cooling this AFM phase becomes more pronounced and clearly visible in the hysteresis loops at $T < 20$ K. Based on theoretical considerations, AFM ordering has been proposed for $Fe^{(III)}$-enriched boundary layers in hemo-ilmenite solid solution with $y \approx 0.7$ (e.g. Lawson *et al.* 1981; Harrison *et al.* 2005). However, our natural hemo-ilmenite ($y = 0.86$) is relatively poor in $Fe^{(III)}$. Since ilmenite-rich solid solutions ($y > 0.9$) exhibit AFM ordering at low temperature as well (*cf.* Ishikawa *et al.* 1985), it is reasonable to attribute the AFM phase to ilmenite-like COA which are depleted in $Fe^{(III)}$.

The occurrence of an AFM phase apart from the FM-ordered CDA in natural hemo-ilmenite puts forward an additional mechanism contributing to the hysteretic properties at $T < 40$ K. An increase in B_c is a characteristic feature of synthetic thin film materials and has been explained with exchange anisotropy (e.g. Berkowitz & Takano 1999). Such anisotropy is associated with the exchange coupling at the interface between a FM and an AFM material. If the AFM anisotropy is low, only a coercivity enhancement is observed, while for large AFM anisotropies a shift in the hysteresis loops should be found (e.g. Nogués & Schuller 1999). In inhomogeneous materials such as natural hemo-ilmenite grains, rough interfaces between the different magnetic nanostructures can be assumed. In our case, the increase of B_c caused by AFM anisotropy cannot be disentangled unambiguously from coercivity changes due to the onset of spin-glass dynamics. The shift in the hysteresis loops (B_{ex}), however, provides clear evidence for exchange bias between the newly ordered AFM areas with the CDA, which show spin-glass dynamics. Continuing blocking of SP clusters in COA increases the AFM contribution and results in an enhancement of these exchange interactions. The increasing shift of the hysteresis loop below 20 K points to the influence of larger AFM anisotropies. At 6 K, the occurrence of both a relatively large $B_c = 244$ mT and $B_{ex} = 40$ mT can be interpreted as local variations of the AFM anisotropy probably caused by structural defects or by the size distribution of the magnetic nanostructures. Meiklejohn & Carter (1959) reported a hysteresis shift for a synthetic hemo-ilmenite ($y = 0.6$) after field cooling. By contrast, the hemo-ilmenite in our soil sample exhibits an exchange bias after cooling in a zero field. Miltényi *et al.* (1999) demonstrated that an exchange bias under such conditions is possible, if the cooling starts from remanent state. This is fulfilled for the natural hemo-ilmenite grains, because the hysteresis loops were performed with decreasing temperature and the FM-ordered CDA carry a remanent magnetization at $T < 200$ K.

5 CONCLUSION

The natural hemo-ilmenite grains of volcanic origin described in our study are composed of two nanostructured phases with different magnetic ordering. These phases, referred to as COA and CDA depending on the local concentration of $Fe^{(III)}$, form a heterogeneous system with a complex magnetic pattern due to superimposed ordering and exchange processes. The combination of static and dynamic magnetization analyses permits an insight into the ordering of the two phases and exchange interactions between them. At $T \approx 220$ K, FM ordering starts in the CDA. Upon cooling the single domain CDA become multidomain. Freezing of the domain walls with a relatively low $Fe^{(III)}$ concentration compared to CDA and the consequent ordering generates competing interactions with previously ordered FM domains. This triggers disorder and frustration which is manifested in the spin-glass dynamics in the FM domains. Blocking of the SP clusters in COA at $T < 40$ K leads to AFM ordering, and the interaction with CDA creates an exchange bias.

The occurrence of exchange bias as well as spin-glass dynamics in the hemo-ilmenite grains is probably an effect of the $Fe^{(III)}$ concentration distribution. While small areas with a low $Fe^{(III)}$ concentration form domain walls, larger COA order antiferromagnetically at low temperature.

Considering the high abundance of hemo-ilmenite as accessory constituent in rocks in combination with its very specific magnetization pattern and its high chemical stability, it has a great potential to be used as mineral tracer to reconstruct landscape development in terms of erosion and mechanical transport. Furthermore, our study demonstrates that it is possible to work with bulk soil samples, if the interference by dominant magnetic remanence carriers (e.g. magnetite) can be minimized.

ACKNOWLEDGMENTS

The authors thank A. Weber, LAC, ETH Zurich for the AC measurements, V. Gramlich, Laboratory for Crystallography ETH Zürich for the XRD data, and Eduard Petrovsky and one anonymous reviewer for their constructive suggestions to the manuscript. This work was supported by the ETH research grant TH02296, and one author (JG) was supported by the University of Nottingham through a Sir Peter Mansfield Fellowship. Contribution 1469 of the Institute of Geophysics, ETH Zurich.

REFERENCES

Arai, M., Ishikawa, Y. & Takei, H., 1985. A new oxide spin-glass system of (1-x) $FeTiO_3$-XFe_2O_3. IV. Neutron scattering studies on a reentrant spin-glass of $79FeTiO_3$-$21Fe_2O_3$ single crystal, *J. Phys. Soc. Jpn.,* **54,** 2279–2286.

Balanda, M. *et al.,* 2005. Magnetic AC susceptibility of stoichiometric and low zinc doped magnetite single crystals, *Eur. Phys. J. B,* **43,** 201–212.

Bennett, L.H. & Della Torre, E., 2005. Analysis of wasp-waist hysteresis loops, *J. Appl. Phys.,* **97,** 10E502.

Berkowitz, A.E. & Takano, K., 1999. Exchange anisotropy—a review, *J. Magn. Magn. Mater.,* **200,** 552–570.

Brown, N.E., Navrotsky, A., Nord, G.L. & Banerjee, S.K., 1993. Hematite-ilmenite (Fe_2O_3-$FeTiO_3$) solid-solution—determination of Fe-Ti order from magnetic-properties, *Am. Mineral.,* **78,** 941–951.

Dickson, D.P.E. & Cardile, C.M., 1986. Magnetic ordering in a montmorillonite observed by ^{57}Fe Mössbauer Spectroscopy at 1.3 K, *Clays &Clay Min.,* **34,** 103–104.

Dormann, J.L., Fiorani, D. & Tronc, E., 1997. Magnetic relaxation in fine-particle systems, *Adv. chem. Phys.,* **98,** 283–494.

Dunlop, D.J. & Xu, S., 1994. Theory of partial thermoremanent magnetization in multidomain grains: 1. Repeated identical barriers to wall motion (single microcoercivity), *J. geophys. Res.,* **99,** 9005–9023.

Fujii, T., Takada, Y., Nakanishi, M. & Takada, J., 2005. Magnetic properties of $Fe_{1.2}Ti_{0.8}O_3/Fe_2O_3$ bilayered films, *IEEE Trans. Magn.,* **41,** 2775–2777.

Gehring, A.U., Guggenberger, G., Zech, W. & Luster, J., 1997. Combined magnetic, spectroscopic, and analytical-chemical approach to infer genetic information for a Vertisol, *Soil Sci. Soc. Am. J.,* **61,** 78–85.

Goulart, A.T., Dejesus, M.F., Fabris, J.D. & Coey, J.M.D., 1994. Characterization of a soil ilmenite developed from basalt, *Hyperfine Interaction,* **91,** 771–775.

Harrison, R.J. & Redfern, S.A.T., 2001. Short- and long-range ordering in the ilmenite-hematite solid solution, *Phys. Chem. Miner.,* **28,** 399–412.

Harrison, R.J., Kasama, T., White, T.A., Simpson, E.T. & Dunin-Borkowski, R.E., 2005. Origin of self-reversed thermoremanent magnetization, *Phys. Rev. Lett.,* **95,** 268501.

Ishikawa, Y., 1964. Superparamagnetism in magnetically dilute systems, *J. appl. Phys.,* **35,** 1054–1059.

Ishikawa, Y., Saito, N., Arai, M., Watanabe, Y. & Takei, H., 1985. A new oxide spin-glass system of (1-x) $FeTiO_3$-XFe_2O_3. I. Magnetic properties, *Phys. Soc. Jpn.,* **54,** 312–325.

Jackson, M., Moskowitz, B., Rosenbaum, J. & Kissel, C., 1998. Field-dependence of AC susceptibility in titanomagnetites, *Earth planet. Sci. Lett.,* **157,** 129–139.

Jönsson, P., 2004. Superparamagnetism and spin-glass dynamics of interacting magnetic nanoparticle systems, *Adv. Chem. Phys.,* **128,** 191–248.

Lagroix, F., Banerjee, S.K. & Moskowitz, B.M., 2004. Revisiting the mechanism of reversed thermoremanent magnetization based on observations from synthetic ferrian ilmenite ($y = 0.7$), *J. geophys. Res.,* **109,** B12108.

Lawson, C.A., Nord, G.L., Dowty, E. & Hargraves, R.B., 1981. Antiphase domains and reverse thermoremanent magnetism in ilmenite-hematite minerals, *Science,* **213,** 1372–1374.

McEnroe, S.A., Harrison, R.J., Robinson, P. & Langenhorst, F., 2002. Nanoscale haematite-ilmenite lamellae in massive ilmenite rock: an example of 'lamellar magnetism' with implications for planetary magnetic anomalies, *Geophys. J. Int.,* **151,** 890–912.

Meiklejohn, W.H. & Carter, R.E., 1959. Exchange anisotropy in rock magnetism, *J. appl. Phys.,* **30,** 2020.

Miltényi, P. *et al.,* 1999. Tuning exchange bias, *Appl. Phys. Lett.,* **75,** 2304–2306.

Nagata, T. & Akimoto, S., 1956. Magnetic properties of ferromagnetic ilmenites, *Geofis. Pura Appl.,* **34,** 36–50.

Nogués, J. & Schuller, I.K., 1999. Exchange bias, *J. Magn. Magn. Mater.,* **192,** 203–232.

Nord, G.L. & Lawson, C.A., 1992. Magnetic properties of ilmenite70-hematite30: effect of transformation-induced twin boundaries, *J. geophys. Res.,* **97,** 10 897–10 910.

O'Reilly, W., 1984, *Rock and Mineral Magnetism*, Blackie, Glasgow and London & Chapman and Hall, New York, 220p.

Pike, C.R., Roberts, A.P. & Verosub, K.L., 1999. Characterizing interactions in fine magnetic particle systems using first order reversal curves, *J. appl. Phys.,* **85,** 6660–6667.

Prévot, M., Hoffman, K.A., Goguitchaichvili, A., Doukhan, J.-P., Shcherbakov, V. & Bina, M., 2001. The mechanism of self-reversal of thermoremanence in natural hemoilmenite crystals: new experimental data and model, *Phys. Earth planet. Inter.,* **126,** 75–92.

Roberts, A.P., Pike, C.R. & Verosub, K.L., 2000. First-order reversal curve diagrams: a new tool for characterizing the magnetic properties of natural samples, *J. geophys. Res.,* **105,** 28 461–28 475.

Schroeder, P.A., Le Golvan, J.J. & Roden, M.F., 2002. Weathering of ilmenite from granite and chlorite schist in the Georgia Piedmont, *Am. Mineral.,* **11–12,** 1616–1625.

Tauxe, L., Mullender, T.A.T. & Pick, T., 1996. Potbellies, wasp-waists, and superparamagnetism in magnetic hysteresis, *J. geophys. Res.,* **101,** 571–583.